ENERGY&FUELS
AN AMERICAN CHEMICAL SOCIETY JOURNAL
VOLUME 16, NUMBER 5 SEPTEMBER/OCTOBER 2002

Articles

Characterization of Metallurgical Chars by Small Angle Neutron Scattering

I. Snook* and I. Yarovsky

Department of Applied Physics, RMIT University, Melbourne, Australia

H. J. M. Hanley and M. Y. Lin

ANSTO, Menai, New South Wales, Australia

D. Mainwaring

Department of Applied Chemistry, RMIT University, Melbourne, Australia

H. Rogers

BHP Minerals Technology, Newcastle Laboratories, Newcastle, New South Wales, Australia

P. Zulli

BHP Steel Research Laboratories, BHP Steel, Port Kembla, New South Wales, Australia

Received April 30, 2001

Small angle neutron scattering (SANS) and nitrogen BET experiments were carried out on coal chars produced in experimental rigs simulating blast furnace pulverized coal injection conditions. From these combined data the main structural features of the chars such as surface area, ratio of open to closed pores and estimates of pore size were obtained. This approach to investigating the pore structure should provide much more detailed and useful data for characterizing industrial carbonaceous samples than traditional methods based only on degree of burnout and/or BET surface area.

Introduction

Pulverized coal injection (PCI) is a procedure in which pulverized coal is injected into the blowpipe/tuyrere of ironmaking blast furnaces (BFs) as a supplementary fuel, replacing a proportion of the metallurgical coke. A number of indicators are used to measure relative coal performance, including the specific energy of the coal (which provides process heat) and the extent of coal combustion (unburnt char solids potentially impact the BFs lower zone burden permeability). The volatile matter content of the coal plays a significant role in both areas of furnace control; generally, as the volatile matter content decreases, the specific energy increases, whereas the extent of coal combustion decreases. The extent of combustion is determined by ash content (which also

* To whom correspondence should be addressed. Email address: ian.snook@rmit.edu.au.

10.1021/ef010107n CCC: $22.00
Published on Web 08/06/2002

affects heat balance), the degree of burnout and the internal porosity of the resultant char.[1]

Porosity is traditionally determined by BET gas adsorption, but it is known that BET results are not always reliable: the adsorption characteristics are influenced by specific surface affinities of the probe gas molecules as well as the inability of the technique to access the enclosed pores[2] that become increasingly available as combustion and/or gasification proceeds. It is, however, also well-known that Small Angle Neutron Scattering (SANS) is an alternative technique to characterize the pore structure of materials[3] since a combination of SANS and the contrast matching experiments has the unique ability to distinguish between open and closed porosity.[4−8] SANS data, however, need to be interpreted with caution since they often cannot yield the structural properties of a porous solid, such as surface area, without the use of models or specific supplementary experimental data. The overall goal of this work was to explore the combined use of this SANS capability with BET measurements in order to characterize metallurgical chars. Specifically, we examined the physical characteristics of char samples produced in combustion testing facilities that simulate injection conditions of a BFs blowpipe and raceway.

Theoretical Background. Small angle scattering measures the intensity $I(q)$ of scattered neutrons as a function of scattering angle θ from the input beam, or alternatively, as a function of the scattering vector $\mathbf{q}$: $q = |\mathbf{q}| = (4\pi/\lambda)\sin(\theta/2)$, where λ is the wavelength of the incident wave. Small angle scattering from porous solids arises from the change in scattering density due to the interface between the solid and the pores. The most common method of analyzing results uses the Porod Model in which one assumes that the porous solid consists of two phases[7,9,10] of constant scattering length density separated by a sharp interface. Thus, we assume that one phase consists of solid of volume fraction ϕ_{solid} and constant scattering length density ρ_{solid}, and the other phase consists of pores of volume fraction ϕ_{pore} and constant scattering length density ρ_{pore}. Then $I(q)$ for small angle scattering can be written as

$$I(q) = 4\pi I_0 V \langle \Delta\rho^2 \rangle \phi_{\text{solid}} \phi_{\text{pore}} \int_0^\infty \{\gamma(r)\sin(qr)/(qr)\}\, r^2\, \mathrm{d}r \qquad (1)$$

where I_0 is a constant, V is the volume of the sample irradiated, $\Delta\rho = \rho_{\text{solid}} - \rho_{\text{pore}}$ is the difference in scattering length density between solid and pores, the brackets $\langle \cdot\cdot \rangle$ indicates averaging over the sample volume, $\gamma(r)$ is the density−density correlation function or characteristic function, and r is the separation between two points in the solid.

All the structural information that may be obtained from a small angle scattering curve—e.g., the structure of the pores—is contained in the characteristic function $\gamma(r)$. In general, however, it is not possible to obtain an unambiguous description of the structure from $\gamma(r)$ alone.[9,10] One can attempt to use a very elaborate, multiparameter model to describe the pores, but this invariably involves obtaining many parameters of unknown physical meaning from limited data.[9,10] This inherent problems in extracting structural data from $I(q)$ is particularly severe in the case of extremely complicated pore structures such as those found in coal and its products.[2] Nevertheless, $I(q)$ can be interpreted provided some straightforward quantities can be evaluated. Two examples are listed below.

First, a useful quantity which may, in principle, be obtained from the scattering curve is the "distance of heterogeneity" or "extent of coherence" l_c introduced by Porod.[9,10] This parameter is a measure of the extent of the porosity and may be calculated from

$$l_c = \{\int_0^\infty \pi q I(q)\, \mathrm{d}q\}/\{\int_0^\infty q^2\, I(q)\, \mathrm{d}q\} \qquad (2)$$

Second, if the characteristic function has a power law dependence on r, for r less than some correlation length ζ, then for q of magnitude greater than ζ^{-1} the scattering curve reduces to a simple power law relationship:

$$I = Bq^{-\alpha} \qquad (3)$$

with a prefactor B and an exponent α. Power law behavior in porous solids in general (hence relevant for the coal and coal based solids discussed here) has been shown to arise from a variety of structural features, for example,

(i) if $2 < \alpha < 3$: from a fractal (irregular) distribution of mass,[11]

(ii) if $\alpha = 4$: from a smooth surface (Porod law),[9]

(iii) if $3 < \alpha \leq 4$: from a fractal (rough) surface (generalized Porod law),[12,13] and

(iv) if $4 < \alpha < 5$: from a fuzzy interface.[14]

For the char samples, the scattering will be dominated by the internal surface areas of the porous chars; therefore, we expect $3 < \alpha \leq 4$. We have found previously that such an analysis gives useful information on the pore structure of coal and coal related materials using minimum assumptions.[11,13,15] We will show that for certain size ranges these pore surfaces can be interpreted as rough, fractal surfaces, in which case the surface area S is not constant but varies with the length of the probe used to measure the surface area

(1) Bodsworth, C.; Bell, H. B. *Physical Chemistry of Iron and Steel Manufacture*, 2nd ed.; Longman: Great Britain, 1972; Chapter 6.
(2) APS Study Group on Coal Utilisation and Synthetic Fuel Production. *Rev. Mod. Phys.* **1981**, *53* (4), Part 2.
(3) Kostortz, G. Treatise on Materials Science and Technology. In *Neutron Scattering*; Academic Press: New York, 1979; Vol. 15, p 227.
(4) Hall, P. J.; Ruiz Machado, W.; Gascon Galan, D.; Barrientos Barria, E. L.; Sherrington, D. C. *Faraday Trans.* **1996**, *92*, 2607.
(5) Hall, P. J.; Berlouis, L. E. A. B.; Mackinnon, A. J.; Wilson, J.; Browning, D.; Dodd, S.; Morris, S.; Jones, P.; Calo J. J. *Alloys Compounds* **1997**, *253*, 195.
(6) Hall, P. J.; Antxustegi, M.; Calo, J. M. *Energy Fuels* **1998**, *12*, 542.
(7) Antxustegi, M. P.; Hall, P. J.; Calo, J. M. *J. Colloid Interface Sci.* **1998**, *202*, 490.
(8) Hall, P. J.; Antxustegi, M.; W. Ruiz, W. *Fuel* **1998**, *77*, 1663.
(9) Giunier, A.; Fournet, G.; Walker, C. B.; Yudowitch, K. *Small Angle Scattering of X-rays*; Wiley: New York, 1955; p 75.
(10) Porod, G. *Small-Angle X-ray Scattering*; Glatter, O., Kratky, O., Eds.; Academic Press: New York, 1982; p 17.
(11) McMahon, P.; Snook, I. *J. Chem. Phys.* **1996**, *105*, 2223.
(12) Bale, H. D.; Schmidt, P. W. *Phys. Rev. Lett.* **1984**, *53*, 596.
(13) Reich, M. H.; Russo, S. P.; Snook, I. K.; Wagenfeld, H. K. *J. Colloid Interface Sci.* **1990**, *135*, 353.
(14) Schmidt, P. W.; Avnir, D.; Levy, D.; Hohr, A.; Steiner, M.; Roll, A. *J. Chem. Phys.* **1991**, *94*, 1474. McMahon, P. J.; Snook, I.; Smith, E. *J. Chem. Phys.* **2001**, *114*, 1578.
(15) Reich, M. H.; Snook, I. K.; Wagenfeld, H. K. *Fuel* **1992**, *71*, 669; Johnston, P. R.; McMahon, P.; Reich, M. H.; Snook, I. K.; Wagenfeld, H. K. *J. Colloid Interface Sci.* **1993**, *155*, 146. Snook, I.; McMahon, P. *Langmuir* **1993**, *9*, 2726. McMahon, P. J.; Snook, I. K.; Moss, S. D.; Johnston, P. R. *Energy Fuels* **1999**, *13*, 965.

Table 1. Physical, SANS, and BET Characteristics of the Chars

char sample	geological source of parent coal	char preparation procedure	degree of burnout %	total open pore surface area, A_o from N_2 BET (m^2/g)	SANS type of curve, from Figure 1	characteristic lengths r_{max} and r_{min} (Å)	SANS estimate of l_c (Å)	SANS % closed pores[a]
B	1	1	6	88.57	1	2000, 300	451	25%
G	1	1	6	30.88	1	2000, 350	439	
A	2	1	32	16.46	2	1800, 180	573	
D	2	1	36	22.33	2	1300, 130	716	<5%
E	3	1	42	19.77	2	1600, 300	562	
C	4	2	77	6.94	3	1800, 480	705	
F	4	2	83	46.25	3	2000, 480	668	<10%
H	5	2	56	15.42	3	1500, 350	771	

[a] Have been estimated for representative samples of low, medium, and high degree of burn out.

according to the formula:

$$S = N_0 r^{2-D_s} \quad (4)$$

where D_s is the surface fractal dimension which is a measure of the surface roughness or irregularity. The dimension lies in the range $2 \le D_s \le 3$. When $D_s = 2$ the surface is smooth, and when $D_s = 3$ the surface is so convoluted that it would fill all space. The parameter N_0 is the surface measure and is the true, probe length independent measure of the extent of the surface. It may be shown, that using eqs 1 and 4, α in eq 3 is given by $D_s = 6 - \alpha$ and the prefactor B is given by[12,13]

$$B = \pi I_0 (\Delta\rho)^2 \, \Gamma(5 - D_s) \sin[(D_s - 1)\pi/2] N_0 \quad (5)$$

where $\Gamma(x)$ is the gamma function.

In short, SANS is able to measure the characteristics of rough surfaces i.e., a roughness factor D_s and a measure of surface extent N_0. It should be noted that this fractal analysis contains the traditional Porod scattering from smooth surfaces as a special case. Then surface area is uniquely defined and is equivalent to N_0. In all other cases, the probe length must be specified in order to quantify the surface area that requires obtaining N_0 from eq 5 then using eq 4.

Finally, eq 1 indicates that the scattered intensity is proportional to the pre-factor $(\rho_{solid} - \rho_{pore})^2$, which, in a dry sample with all pores full of air, is nonzero. If, however, we immerse the sample in a liquid whose scattering length density equals that of the sample, and if all the pores were open and accessible to the liquid, the scattering would decline to background. Conversely, any nonzero scattering under these circumstances would arise from pores that are closed. In practice, this manipulation of the scattered intensity or contrast matching, is controlled by immersing the sample in various combinations of hydrogenated and deuterated liquids.

Experimental Section

Materials. The chars used for these feasibility studies were prepared from parent coals obtained from different geological sources and from two different PCI combustion test facilities. Specifically, samples arbitrarily labeled A, B, D, E, and G were obtained[16,17] from tests carried out at 1100 and 1300 °C in a cylindrical combustion test section of 110 mm internal diameter to give an actual blast velocity of 40 ms^{-1}. The combusting coal plume was fully confined/restrained by the combustion test section. This procedure is denoted as procedure 1 in Table 1.

The other group of chars, samples C, F, and H, was produced in tests conducted in a cylindrical test section of 300 mm internal diameter. The blast of 1200 °C passed through a 70 mm diameter ceramic tuyere into the combustion test chamber. Coal was injected at the entry of the tuyere and the combustion plume expanded into the combustion test section. This set up (procedure 2, Table 1) leads to a much lower particle density in the combustion plume, and thus higher oxygen availability at the surface of the combusting particles.

The resultant chars from both procedures were characterized by the extent of coal combustion or degree of burnout (Table 1). The term "coal burnout", or fractional burnout, refers to the proportion of the coal carbonaceous material removed in the combustion process. Clearly, burnout is a function of how the combustion process is undertaken. The results reported here for the chars are calculated on the basis of full conservation of the ash between the precursor coal and the product char.

SANS Measurements. The small angle neutron scattering experiments were carried out at the National Institute for Standards and Technology, Center for Neutron Research (Gaithersburg, USA). All samples were powders and loaded on a constant volume basis into cylindrical sample holders with two flat quartz windows with a neutron path length of 0.1 cm. Initial data were obtained from the 8 m SANS instrument configured at a sample−detector distance of 3.6 m, off-center angle of 3.5°, with a central incident neutron wavelength of 8 Å (25% spread), a sample−detector distance of 3.6 m, off-center angle of 0 degree, with a central incident neutron wavelength of 16 Å (also 25% spread). The total momentum transfer range probed combining both configurations was $0.0045\ Å^{-1} < q < 0.13\ Å^{-1}$. The 8 m tests were repeated, and the q range extended, by carrying out further experiments on the 30 m NG7-SAN configured to three settings. With incident neutrons of wavelength of 6 Å (10% spread) and a sample-to-detector distance of 15.3 m, the first setting covered a q range of 0.002−0.04 $Å^{-1}$. With incident neutrons of wavelength of 6 Å (10%) and a sample-to-detector distance of 2 m distance, a second setting covered q from 0.016 to 0.3 $Å^{-1}$. The third setting set the incident wavelength to 5 Å (10%) and the sample-to-detector distance of 1.5 m to give data for q between 0.04 and 0.68 $Å^{-1}$.

All data were collected by an area detector and then reduced by subtracting the effects of background (blocked beam at the sample position), empty cell, and scaled to an absolute value of scattering cross section per unit volume. The data are presented as the one-dimensional intensity (cm^{-1}) by circular averaging.

Contrast Matching Measurements. As noted in the previous section, immersing a given powder sample in various solvents will allow the neutron contrast to be controlled and

(16) Haywood, R. J.; McCarthy, M. J.; Truelove, J. S.; Mason M. B.; Thomson, A. D. *Australian Symposium on Combustion and Fourth Australian Flame Days*; Adelaide, Australia, 1995.

(17) Zulli, P.; McCarthy, M. J.; Horrocks, K. S. R. *Aust. Coal Rev.* **1996**, *1*, 42.

hence give information on the proportion of closed versus open pores. Here, our approach was very simple and preliminary: details on the technique as applied to carbonaceous substances are given by, for example, Hall and co-workers.[4−8]

To a first approximation char, corresponds to pure carbon and has a typical carbon scattering length density of 5.7×10^{10} cm^{-2} and thus would be contrasted out by immersing in deuterated toluene which also has a scattering length density of 5.7×10^{10} cm^{-2}. For the matching experiments, we selected samples B, D, and F as representatives of the groups discussed later, and for each given sample made up pastes with toluene, deuterated toluene, and a mixture of toluene and deuterated toluene. The samples of equal volume of solids were loaded in 0.1 cm path length quartz cells, placed in the neutron beam and scanned at various times (immediately after preparation, several hours later, and 2 days later) to observe if any change in scattering intensity occurred. It turned out that at the ambient temperature and pressure of the experiments, the systems equilibrated after 20 h.

Experiments were run on the NG7 at only the low-q setting (0.002 Å$^{-1} < q < 0.04$ Å^{-1}) and some limited runs were carried out on the 8 m SANS set at 12 Å (15% spread) with a sample−detector distance of 5.0 m.

Nitrogen BET Measurements. Outgassing and measurements of nitrogen adsorption isotherms were carried out using a Micromeretics ASAP 2010 automated surface area analyzer. Samples were outgassed at 623 K under vacuum for 24 h to a final pressure of 10MPa, prior to bringing to liquid nitrogen temperature. The dead volume was measured separately for each sample using helium gas. Nitrogen gas used was better than 99.99% purity. During isotherm determination, each dose of gas was allowed to completely equilibrate which was determined by monitoring pressures at 45 s intervals.

Results and Discussion

Overall Structural Features of the Samples. Background subtracted scattering intensities $I(q)$ for the samples are presented in Figure 1. It was immediately noted that the SANS scattering curves could be grouped into three distinct categories according to their basic features which are detailed below. Thus the SANS and BET results for the dry chars summarized in Table 1 were grouped according to this preliminary classification. As is normally done, the high q limiting intensities, corresponding approximately to the incoherent scattering, were subtracted from the background subtracted intensities to give I_{corr} which was used for subsequent analysis.

The experimental transmissions for all samples were approximately 0.7 at the wavelength of 6 Å. The calculated transmission for carbon alone would be 0.95 and thus the samples must contain some other elements. Provided that these chars did not contain any strong absorbers, the difference in transmission should be due to hydrogen containing compounds and/or hydroscopically adsorbed water. The transmission drop due to hydroscopic water alone, however, is inconsistent with the relatively low incoherent background. Hence, we conclude that some other hydrogen containing compounds are present in the samples.

The results for char samples B and G presented in Figure 1 show a linear region for $q < 0.05$ Å^{-1} with a largely flat region at higher q and a slight maximum at approximately $q = 0.3$ Å^{-1}. The curves for samples A, D, and E are characterized by higher overall intensity as well as by a less distinct transition from one scattering regime to another, as can be seen from the more

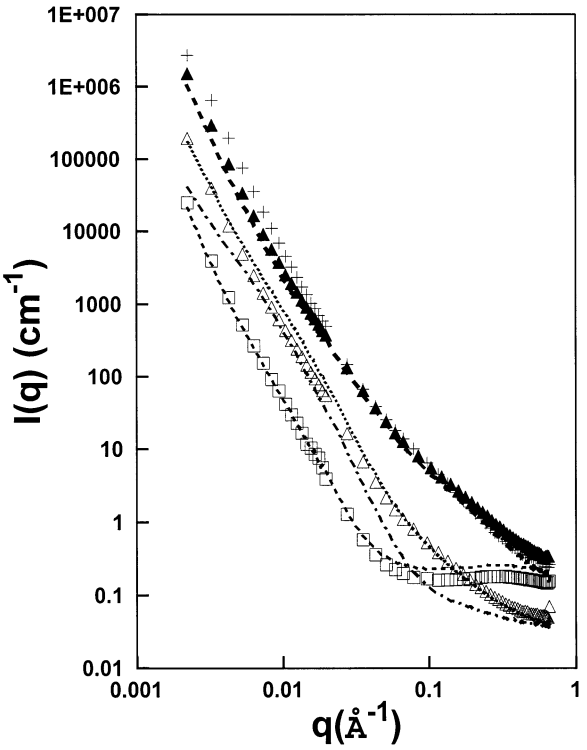

Figure 1. Background subtracted SANS intensity $I(q)$ versus the magnitude of the scattering vector **q** for all samples. The curves for the samples are labeled as follows: Group 1, B(□) and G(- -); Group 2, A(· ·), D(△), and E(● − ●); and Group 3, C(+), F(▲), and H(- - -). The curves for group 3 in Table 1 (samples C, F, and H) have been off set by a factor of 10 for clarity.

continuous overall shape of the curves. It should be noted that sample E, although having a similar scattering curve to A and D, shows a more pronounced transition. The curves for samples C, H, and F are characterized by a very smooth transition from one linear region to another. The overall intensity is similar to the sample group A, D, and E.

As the log−log plots (Figures 2−4) showed a linear region for a limited range of q values indicating that this scattering regime may be interpreted as arising from fractal surfaces, i.e., surfaces having no characteristic length but having dimensions only in a limited size range. Since, however, the plots show linear behavior only over this limited range, a fractal approach will not provide a complete description of our samples. In fact, this suggests that these samples may have some characteristic lengths that cannot be accounted for by a fractal analysis. To address this problem we subtracted an estimate of the fractal contribution to the scattering I_F, obtained by fitting the linear region of the log/log plots from the experimental intensities I_{corr}. We then analyzed the resultant difference, $\Delta I = I_{corr} - I_{fractal}$.

We identifid the q value at which ΔI become significant by arbitrarily choosing the value of q at which ΔI becomes10% of I_{corr}. Two q values are then identified, one at low q, q_{min}, and one at intermediate q, q_{max}. Using $r = 2\pi/q$ the corresponding characteristic lengths are presented in Table 1.

The significant value of the ΔI arises from two effects.

(1) At small q, from the scattering by some objects of characteristic length >2000 Å which is beyond the

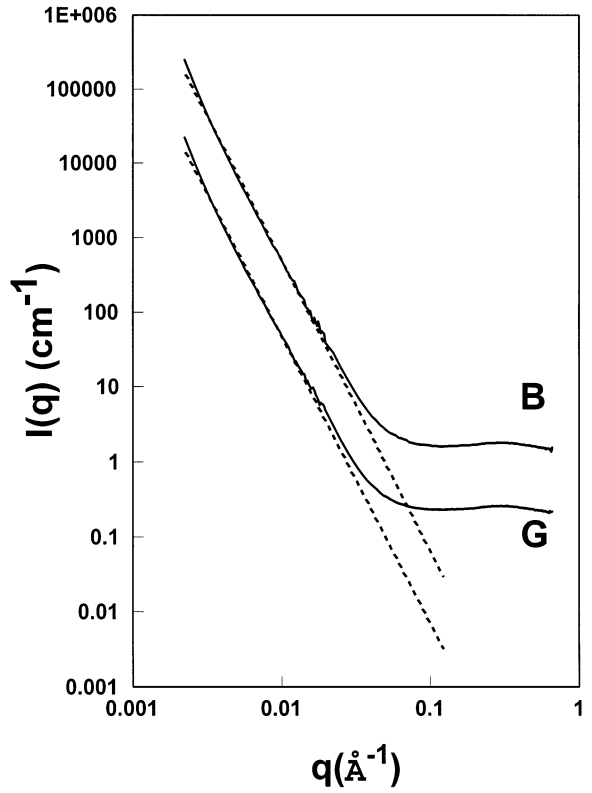

Figure 2. SANS intensity $I(q)$ versus the magnitude of the scattering vector q for samples for samples B and G together with the fractal fits. The data for sample B has been multiplied by a factor of 10 for clarity.

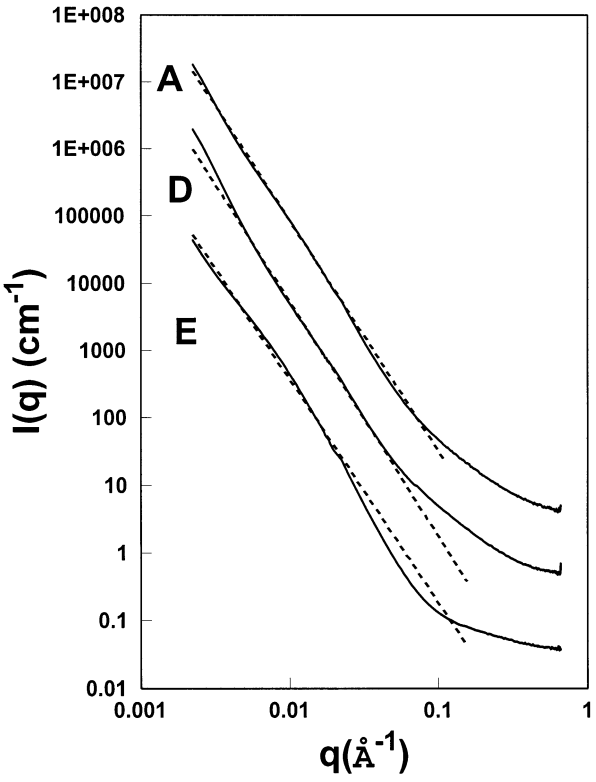

Figure 3. As in Figure 2 but for samples A, D, and E together with the fractal fits. The data for sample A has been multiplied by a factor of a hundred and the data for sample D by a factor of 10 for clarity.

resolution of our measurements and therefore we cannot analyze it in any more detail.

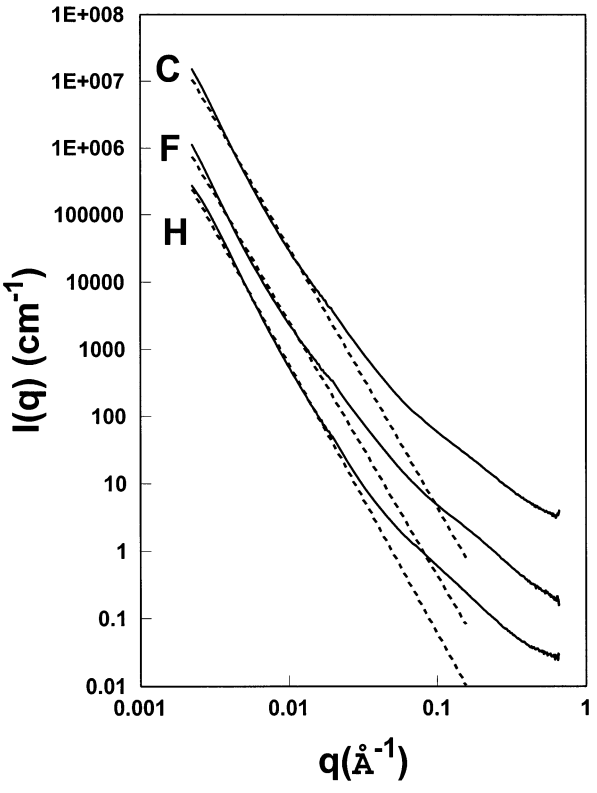

Figure 4. As in Figure 2 but for samples C, F, and H together with the fractal fits. The data for sample C has been multiplied by a factor of a hundred and the data for sample F by a factor of 10 for clarity.

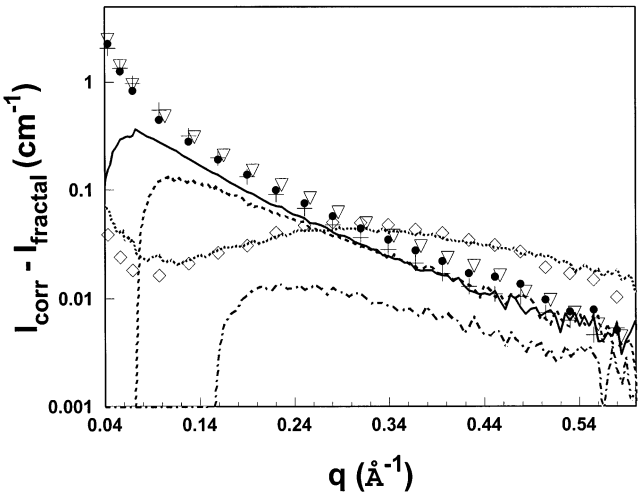

Figure 5. The difference, ΔI in the total intensity (corrected for incoherent scattering) and the fractal fits for large q. The samples are labeled as follows B(• •), G(◇), A(- -), D(—), E(— • -), C(▽), F(●●), and H(+). The falloff in intensity at small q is not considered significant and merely results from our analysis procedure.

(2) At moderate to large q, from nonfractal smaller scale porosity, i.e., characteristic lengths less than approximately 300 Å.

To develop a better picture of the small scale porosity in the samples we performed a more detailed analysis of the ΔI at moderate to large q. We plotted ΔI at moderate to large q, as presented in Figure 5.

Analysis of these plots shows the following.

(1) For type 1 samples, i.e., B and G, ΔI has a peak at $q \approx 0.3$ corresponding to a length of approximately

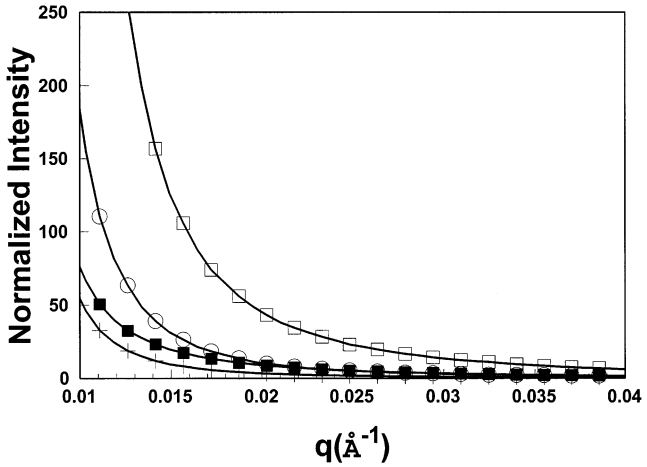

Figure 6. SANS data for the d-toluene wetted samples, sample B (○), D (+) and F (■). The intensities have been normalized with respect to the data for the dry samples (□).

20 Å. This indicates the existence of either particles or particle spacings of this characteristic length.

(2) For type 2 samples, i.e., A, D, and E, ΔI shows a decay for q greater than q_{max} is close to exponential with no discernible peaks being present. This most probably indicates that there is a continuous distribution of pore dimensions with no one characteristic length.

(3) For type 3 samples i.e., C, F, and H, ΔI also shows a decay for q greater than q_{max} but the analysis indicates that here it is a power law decay with no discernible peaks being present. This once again indicates that the distribution of pore dimensions is probably continuous with no obvious characteristic length.

Closed Porosity. The relative intensity plots of samples in *d*-toluene are shown in Figure 6 where we have normalized the scattering curves for each wetted sample with respect to the data for the dry sample. To a first approximation, the extent of open porosity is proportional to the drop in intensity measured between the dry and the toluene-wetted samples. Hence, sample B clearly has more closed pores than the others. The discrepancy between F and D is not so marked but obviously the scattering from D is less. A more detailed analysis of these curves would require a better check of the contrast point of the char samples: here we have assumed that the chemical make up of all three is the same and that the scattering length density[6,7] is 5.7×10^{10} cm^{-2}. While this cannot be strictly true, the sample transmissions and incoherent background suggest that the main difference between the samples lies in their hydrogen content. The scattering power of hydrogen and *d*-toluene is small compared to that of carbon. The proportion of inorganic compounds in each sample is small and roughly the same. Hence, our choice to use the carbon scattering length density for all three samples is practical.

An approximate estimate of the percentage of closed pores p follows by applying the following expression:

$$I(q) \sim (\Delta\rho_{solid})^2 S_{solid}(q)p + (\Delta\rho_{pore})^2 (1-p) S_{pore}(q) + 2(1-p)p S_{solvent-pore}(q)\, \Delta\rho_{solid}\Delta\rho_{pore} \quad (6)$$

where $\Delta\rho$ values are the scattering length density difference between the solid and solvent and the pore and solvent. We take the scattering from the pore to be that of air. For dry samples $\Delta\rho_{pore}$ is zero; for samples in *d*-toluene, $\Delta\rho_{solid}$ is zero. At low values of q the forms of the structure factors $S(q)$ are similar, Figure 1. Our estimates of closed porosity are given in Table 1. We confirmed that our estimates of porosity are reasonable from measurements using the 50/50 mixture of *d*- and h-toluene. The results indicate that the closed porosity of the first group are about 25%; those of the second group less than 5%, and those of the third group are less than 10%. The results are approximate but indicate realistically the relative porosity of the three types of chars.

Distance of Heterogeneity. We have also used eq 2 to estimate the "distance of heterogeneity" or "extent of coherence" l_c introduced by Porod. Values of l_c are shown in Table 1. Strictly both of the integrals in eq 2 should be evaluated over all values of q. Here, we can only evaluate the integrals over a finite range of q but we can still obtain meaningful relative values of l_c and, thus, enable a comparison of the different solids. The values in Table 1 indicate that this distance of heterogeneity is smaller for sample B and G than for the other solids.

Surface Areas. As mentioned previously the surface areas for a fractal surface can only be defined when the probe radius is identified (eq 4). Once the probe radius r is specified, the surface area can be calculated using the following equation:[13]

$$S(r)/V = Br^{2-}D_s/(2\pi\Delta\rho^2 F(D_s)) \quad (7)$$

where $F(D_s) = \Gamma(5 - D_s)\sin[(3 - D_s)\pi/2]$. All the other symbols are previously defined.

Assuming that the average bulk packing density of the samples was $d = 0.39$ g/cm3, the left-hand side of the eq 7 can be converted to the surface area per unit mass using $S/M = S/Vd$ where M is the mass of the sample.

Since the fractal analysis only describes the SANS data for dimensions less than r_{max}, we estimated the fractal contribution to the pore surface area A_F using this probe length and obtained the surface area values for our samples that are presented in Table 2.

The BET surface areas uses the N_2 molecule whose dimensions are smaller than the smallest dimensions probed by our SANS measurements and thus these areas should give an estimate of the total surface areas of the open pores A_o. Hence the difference $A_o - A_F$ gives us a measure of the surface area A_s for pore dimensions less than r_{max} provided the pores are open. The results of this analysis are contained in Table 2, and as can be seen, a majority of the surface area of the pores is contributed by pores of dimension less than r_{max} except for char A. But even in this case the small pores contribute nearly one-half of this surface area. The analysis is very approximate for samples B and G where 25% of the pores are closed. A complete analysis of the small pore structure for B and G would require further work. This, is not justified here, however, since samples with such a low burn out and a high level of closed porosity are of no practical value for the metallurgical applications in question.

(18) Ruike, M.; Kasu, T.; Setoyama, N.; Suzuki, T.; Kaneko, K. *J. Phys. Chem.* **1994**, *98*, 9594.

Table 2. Surface Area Analysis of Chars

char sample	SANS estimate of D_s	SANS estimate of N_0 ($m^{D_s} \times 10^{-7}$)	cut-off length on fractal behavior r_{max} (Å)	surface area A_F of fractal surface for $r < r_{max}$ (m^2/g)	surface area A_S of small pores (m^2/g)	% surface area contained in small pores
B	2.14	1.67	300	0.30	88.27	99.7
G	2.18	2.14	350	0.29	30.59	99
A	2.57	465	180	9.36	7.10	43
D	2.53	217	130	6.58	15.75	71
E	2.69	531	300	4.04	15.73	80
C	2.14	11.9	480	1.99	4.95	71
F	2.23	15.5	480	1.48	44.77	97
H	2.0	9.96	350	3.83	11.59	75

Conclusions

In this paper, a study was undertaken of the porosity of a selected range of char samples by a combination of SANS, contrast matching and BET measurements. These samples were produced from different combustion facilities simulating pulverized coal injection into an ironmaking blast furnace.

The SANS measurements combined with contrast matching were used to distinguish between open and closed porosity and it was found that the samples with medium to high burnout contained very little closed porosity, while the samples with very low burnout contained a considerable percentage of closed pores.

For q vectors of magnitude less than a value q_{max}, the SANS data could be interpreted as arising from scattering by fractal pore surfaces having dimensions greater than $r_{min} = 2\pi/q_{max.}$ This enabled us to make an estimate of the surface area of this fractal region A_F. The BET results gave an estimate of the total surface area of the open pores A_o. The difference between A_o and A_F gave us a measure of the surface area of small pores of dimensions less than r_{min}. In all cases a large proportion of the pore surface area was shown to be due to these small pores.

We note that the degree of burn out is usually used as an indicator of coal behavior in metallurgical applications. However, we have shown that the degree of burnout is not simply related to any of the measured structural characteristics of the chars. Thus, for a complete understanding of these materials and to simulate the chemical and physical processes which are intimately related to pore surface, their structure will need to be modeled in a more sophisticated way.

Future SANS work can be envisaged for evaluating the variation in internal porosity of coals and char samples, produced from single coal sources under similar processing conditions. This can potentially lead to better ways of evaluating suitability of coals for BF applications.

Acknowledgment. We would like to acknowledge the help of Dr J.N. Watson (ANSTO) for his contribution to the SANS measurements. Part of the work was carried out under an ANSTO/NIST SANS agreement. SANS data were taken on the NIST SANS spectrometers at Gaithersburg, Maryland.

EF010107N